JACS
JOURNAL OF THE AMERICAN CHEMICAL SOCIETY

Article

pubs.acs.org/JACS

Phthalocyanine–Perylenediimide Cart Wheels

Javier Fernández-Ariza,[†] Rafael M. Krick Calderón,[‡] M. Salomé Rodríguez-Morgade,*[,†] Dirk M. Guldi,*[,‡] and Tomás Torres*[,†,§]

[†]Departamento de Química Orgánica, Universidad Autónoma de Madrid, Cantoblanco, 28049 Madrid, Spain

[‡]Department of Chemistry and Pharmacy & Interdisciplinary Center for Molecular Materials (ICMM), University of Erlangen–Nuremberg, Egerlandstraße 3, 91058 Erlangen, Germany

[§]IMDEA-Nanociencia, c/ Faraday 9, Cantoblanco, 28049 Madrid, Spain

Supporting Information

ABSTRACT: The electronic features of Zn(II) and Ru(II) phthalocyanines (Pcs) have been modulated by direct peripheral attachment of up to eight ferrocenes. The presence of peripheral ferrocenes noticeably impacts the electronic properties of the corresponding ZnPc and RuPc complexes **7**, **12** and **9**, **15**, respectively—a notion that is supported by optical spectroscopy with bathochromic shifts of up to 8–10 nm per ferrocene unit. Cyclic voltammetry and optical spectroscopy reveal long-distance (10–11 bonds) electronic interaction between ferrocene units. The ZnPc and RuPc complexes have been integrated into a series of orthogonal, supramolecular bis(phthalocyanine)–perylenediimide electron donor–acceptor conjugates, **2a,b** and **3a,b**. In these cart-wheel-shaped arrays, coordination of ditopic perylenediimide **16**, containing two pyridyl substituents at its imido positions, enabled selective interactions with the metal centers of phthalocyanines **7**, **12**, **9**, and **15**. The presence of ferrocenes in, for example, Zn complexes **2a** and **3a** triggers a fast energy transfer from the excited-state PDI to ZnPc. In the RuPc-PDI conjugates, substitution with ferrocenes produces a slight acceleration of the charge separation upon photoexcitation of the PDI chromophore. However, charge recombination is accelerated by 2 orders of magnitude in ferrocene-containing conjugates when compared to that in the analogous *tert*-butyl-substituted array **1b**.

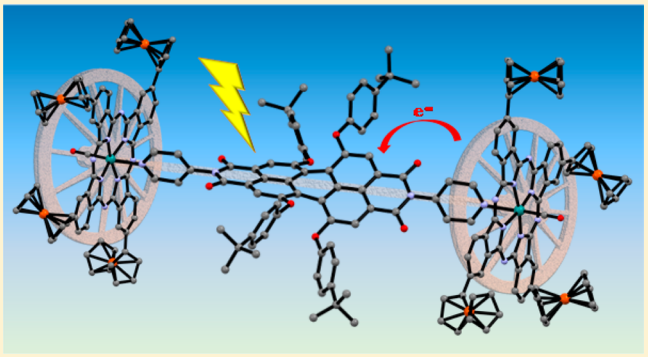

INTRODUCTION

The Sun is the main energy supplier for terrestrial existence. In this context, photosynthesis is the method evolved in nature to capture solar energy and store it in the form of fuel based on energy-rich carbohydrates. Most of the energy consumed by living organisms comes from the *on demand* metabolism of these carbohydrates, generating high-energy molecules to be used by the cell. At the end, oxygen is reduced to water, which, in turn transports the energetic electrons involved in this process. In this perfect and intricate mechanism, both photosynthesis and respiration are complementary, namely, each process uses the ashes—water, oxygen, and carbon dioxide—produced in the other one. Therefore, it is hardly surprising that mimicking nature by harvesting and converting sunlight, as a method to provide clean, reliable, and affordable energy, has become an attractive goal in the field of renewable energy.[1,2]

Chemical strategies to undertake the design and study of photosynthetic systems are based on a modular approach, with individual components for light absorption, energy transfer, electron transfer, redox catalysis, etc. These are typically investigated separately, optimized in performance, and assembled with suitable architectures into single devices. Although complexity is inevitable due to multifunctional requisites, this strategy offers the benefits of simple iterations by means of chemical synthesis, followed by the study of individual components independently.[3]

Designing electron donors and acceptors has become crucial in the fields of solar photochemistry and solar energy conversion. Such systems assist in mimicking the basics of at least one of the photosynthetic key steps, namely photoinduced charge separation.[4−6] Electron donor–acceptor systems are also of interest in the area of molecular photovoltaics,[7] which convert the energy gathered in the photogenerated radical ion pair states into electrical power. The excited-state energy of the electron donor is essential, as it should be reductive enough to transfer one electron to the electron-accepting counterpart. In this context, besides *nature-inspired* porphyrin–quinone arrays,[8] other electroactive units and/or chromophores have been explored.[1,4,9] Among the latter, phthalocyanines (Pcs)[10] stand out for applications in solar technologies. First, they display strong absorptions in the visible region, with a maximum around 700 nm, where the maximum of the solar photon flux

Received: July 19, 2016
Published: August 31, 2016

DOI: 10.1021/jacs.6b07432
J. Am. Chem. Soc. 2016, 138, 12963–12974

Chart 1. Structures of 1−3

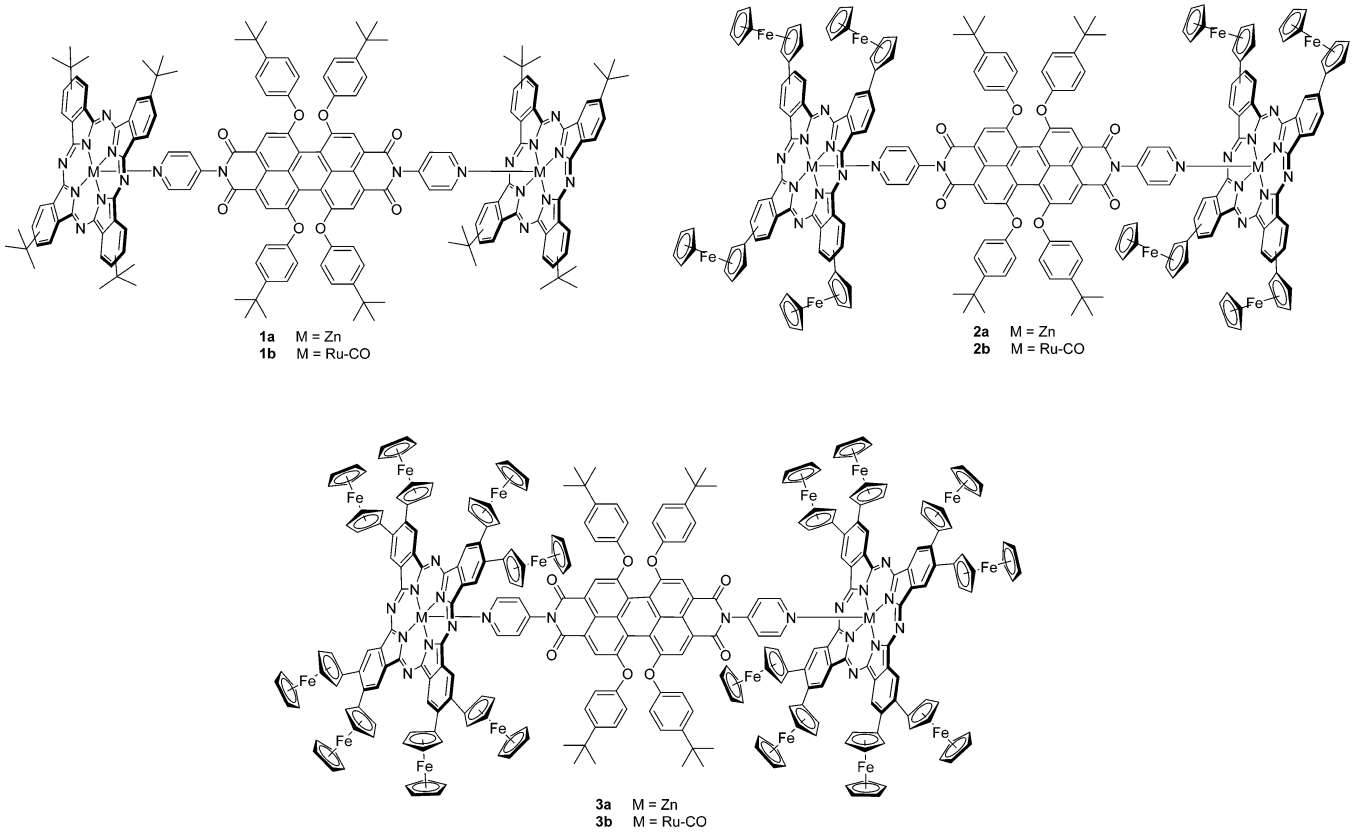

occurs.[11] Second, their large, conjugated π-systems are suitable for efficient electron-transfer processes.[12] Third, Pcs can be endowed with a range of redox potentials by simple introduction of different central metals and/or functionalization at the periphery.[13] Taking the aforementioned in concert, they can be designed to act as electron donors or acceptors, depending on the selected counterpart. Despite such functional duality, these macrocycles are usually designed to behave as electron donors.[14]

In the context of electron acceptors, fullerenes have often been preferred as Pc complement[15] in either covalently linked phthalocyanine−fullerene conjugates[16,17] or supramolecularly assembled phthalocyanine−fullerene hybrids.[18,19] Some of these architectures also exhibit promising performance as constituents in photovoltaic devices.[12c,15,17a,20]

Recently, we[21] and others[22] have established perylenediimides (PDIs) as effective oxidizing components in Pc-based donor−acceptor hybrids. In particular, the two chromophores, namely Pc and PDI, were attached through different means through Pc axial/peripheral positions and PDI imido/bay regions, using a variety of chemical connections such as metal coordination or hydrogen bonds, as well as conjugated and non-conjugated covalent linkages. One of our own approaches involves an orthogonal, supramolecular bis(phthalocyanine)−perylenediimide electron donor−acceptor conjugate.[21a] This cart-wheel array was assembled by the strong coordination of a perylene-(bis)imide dye [BPyPDI], endowed with two pyridine groups at the imido positions, to the central metals of two ruthenium(II) carbonyl phthalocyanines, [Ru(CO)Pc] (see Chart 1, compound **1b**). Here, the presence of nodes at the imido nitrogens in the HOMO and LUMO of PDIs disrupts the electronic communication between the Pc and the PDI.[23] The design offers several advantages from a synthetic point of view.

First, the Pc−PDI hybrid is prepared through a convergent strategy, where the last step consists in the assembly of the two chromophores. As such, the physicochemical features of Pc and PDI are individually tunable through chemical synthesis. Second, A_4-type Pcs are applicable, so a low-yielding, statistical condensation is avoided. Third, PDI derivatives are symmetrically substituted at the imido positions, and, in turn, tedious synthetic protocols are not necessary. Fourth, the geometry and stoichiometry of the array are easily controlled by using Ru(II)Pcs bearing a strong carbonyl ligand at one of the two ruthenium axial coordination sites. The latter prevents the formation of mixtures by exclusively directing the PDI to the other Pc axial position.[21a,d,24]

In this work, we aimed at optimizing the photophysical response of [Ru(CO)Pc]-[BPyPDI]-[Ru(CO)Pc] (**1b**) by the preparation of new cart-wheel-type hybrids from new modified Pcs. Within this model, Pcs bearing different metal ions should render electron donor−acceptor conjugates linked with different strengths. Weaker electron donor−acceptor associations could slow down the charge recombination process by dissociation after electron transfer. In this respect, we expected different behaviors for ZnPc and RuPc complexes, as components of cart-wheel systems **1**−**3** based, on one hand, on the different strength of the pyridyl−Ru and pyridyl−Zn coordination bonds and, on the other hand, on their different abilities to stabilize triplet excited states.

A potent strategy for the design of electron-donating Pcs entails their peripheral functionalization with, for example, metallocenes, such as ferrocene. Notable is the electrochemical reversibility of the ferrocenium/ferrocene couple. Besides,

DOI: 10.1021/jacs.6b07432
J. Am. Chem. Soc. 2016, 138, 12963−12974

Scheme 1. Synthesis of Tetraferrocenylphthalocyanines [$ZnFc_4Pc$] (7) and [$Ru(CO)Fc_4Pc$] (9)

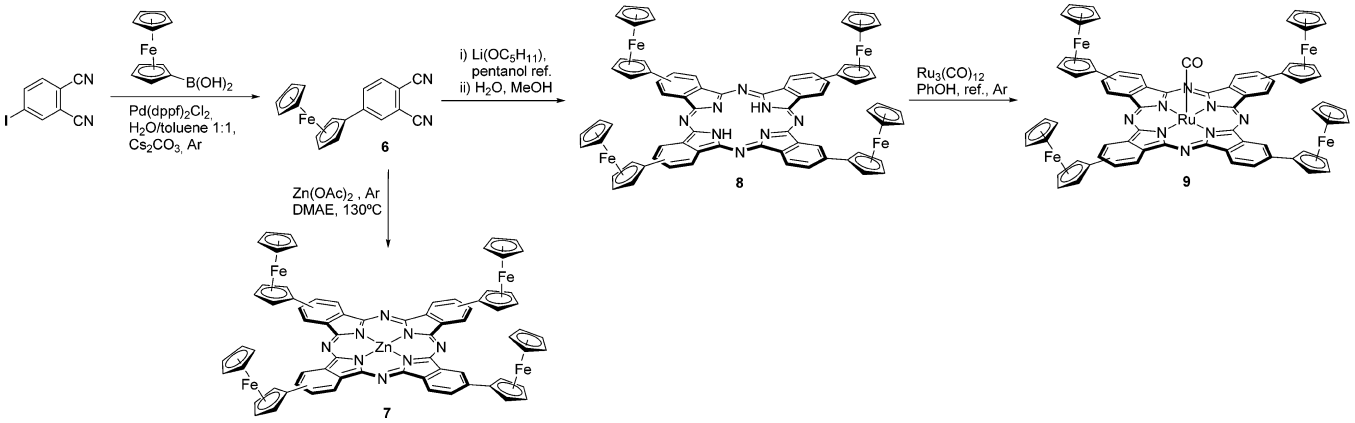

Scheme 2. Synthesis of Octaferrocenylphthalocyanines [$ZnFc_8Pc$] (12) and [$Ru(CO)Fc_8Pc$] (15)

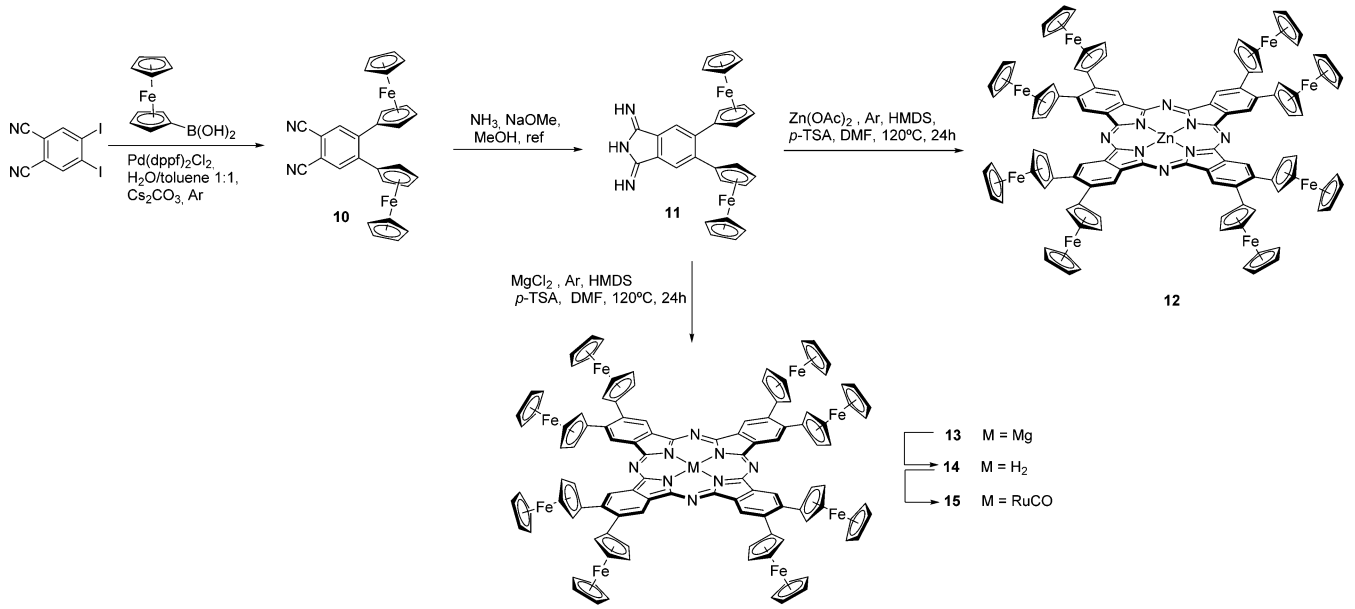

ferrocenes interact with π-conjugated systems both through the cyclopentadienyl anion and through the metal orbitals,[25] and this should enrich the Pc with further redox processes.[26] The role of these secondary electron donors is to reduce the generated Pc radical cation through a subsequent electron shift and, thus, to stabilize charge separation.[6d,27]

We report herein the synthesis and photophysical characterization of Pcs bearing four and eight ferrocenes directly attached to the periphery of Ru(II)Pcs and Zn(II)Pcs. In a second stage, these Pcs are assembled into the corresponding cart-wheel Pc-PDI-Pc hybrids **1**–**3** (Chart 1) of different nature and compared in terms of their abilities to generate long-lived charge-separated states.

RESULTS AND DISCUSSION

Synthesis of Phthalocyanines. Tetra-*tert*-butylphthalocyanines containing Zn(II) (**4**)[28] and Ru(II)(CO) (**5**) were prepared using reported procedures.[21] The synthesis of Pcs is usually carried out by cyclotetramerization reaction of phthalonitrile derivatives. A synthetic method for the preparation of 4-ferrocenylphthalonitrile **6** in 45% yield, consisting in reacting ferrocenium chloride with 4-diazonium-phthalonitrile bisulfate, has been reported previously by C. C. Leznoff.[29] We have prepared **6** by a different procedure, involving a Suzuki cross-coupling reaction of 4-iodophthalonitrile[30] with ferroceneboronic acid (Scheme 1). [$ZnFc_4Pc$] (**7**) was then obtained in 25% yield by template cyclotetramerization of phthalonitrile **6** in the presence of zinc acetate (Scheme 1). The analogous [$Ru(CO)Fc_4Pc$] (**9**) was achieved in 24% overall yield through metalation of the corresponding phthalocyanine free base with ruthenium dodecacarbonyl in boiling phenol, following a reported procedure (Scheme 1).[21a] Both Pcs **7** and **9** were obtained and further used as a mixture of four regioisomers arising from the unsymmetrical substitution of phthalonitrile **6**.[31]

In order to work with single regioisomers and render their characterization easier, octasubstituted Pcs were also prepared. Hence 4,5-bisferrocenylphthalonitrile **10** was synthesized by Suzuki cross coupling of 4,5-diiodophthalonitrile[32] with ferroceneboronic acid (Scheme 2). However, **10** failed to afford any Pc under either of the above-described cyclotetramerization conditions. This is not surprising taking into account the electron donating character of the ferrocene units, which should reduce the reactivity of the phthalonitrile derivatives toward Pc formation. A common strategy to obtain

DOI: 10.1021/jacs.6b07432
J. Am. Chem. Soc. 2016, 138, 12963–12974

more reactive precursors consists in the preparation of the corresponding diiminoisoindolines. Therefore, **10** was treated with ammonia in methanol in the presence of sodium methoxide, giving **11** in 72% yield. Cyclotetramerization of **11** to afford octaferrocenylphthalocyanines was best accomplished in the presence of hexamethyl disilazane (HMDS). This reagent has been postulated to behave as nucleophilic reagent and source of nitrogen, activating phthalonitriles, phthalimides, or phthalic anhydrides by converting them into diiminoisoindoline derivatives, which, in turn, undergo intermolecular condensation.[33] In our case, our starting material is already a diiminoisoindoline. However, the use of other typical cyclotetramerization conditions such as heating in lithium/magnesium alcoholate, or in dimethylaminoethanol in the presence of metal salts, or in pentanol/octanol in the presence of DBU, either failed or rendered only marginal yields of Pcs. Therefore, [ZnFc$_8$Pc] (**12**) was prepared in 20% yield by cyclotetramerization of **11** in DMF, in the presence of zinc acetate, HMDS, and *p*-toluensulfonic acid (Scheme 2). Likewise, free base Pc **14** was achieved under the same reaction conditions but using magnesium chloride as metal salt, followed by demetalation with TFA. Metalation with trisruthenium dodecacarbonyl in phenol afforded [Ru(CO)-Fc$_8$Pc] (**15**) (11% yield over three steps, Scheme 2).

Phthalocyanines **7**, **9**, **12**, and **15** displayed in MS (MALDI-TOF) their corresponding isotopic patterns for $[M]^+$ at m/z = 1312, 1368, 2050 and 2114, respectively. Moreover, carbonylruthenium Pcs **9** and **15** exhibited in their IR spectra very intense bands at 1962 and 1963 cm^{-1}, respectively, characteristic of the carbonyl stretching.

Judging by their well resolved ^{1}H NMR spectra, tetra- and octaferrocenylphthalocyanines do not seem to aggregate notably in solution. This reduced aggregation arises from their peripheral substitution by means of bulky groups. Owing to the regioisomeric mixture and their limited solubility, tetrasubstituted Pcs **7** and **9** show broader signals. Specifically, the aromatic isoindole protons appear at 9.2 and 8.2 ppm (Pc **7**, Figure S15) and 9.45, 9.30, and 8.83 ppm (Pc **9**, Figure S21), while signals at 4.6 and 4.2 ppm account for the ferrocene subunits. Octasubstituted Pcs **12** and **15** are more soluble, single regioisomers; hence, they show sharper and well-resolved signals in ^{1}H NMR. In particular, **12** and **15** display their isoindole proton as a singlet at 9.94 and 9.86 ppm (Figures S26 and S33), respectively, together with the ferrocene protons appearing at 4.6 and 4.4 ppm.

Assembly of Cart-Wheel Ru(II) Complexes 1b, 2b, and 3b. The central PDI unit was endowed with bulky *tert*-butylphenoxy-groups at the four positions of the bay region to ensure solubility and prevent aggregation.[34] *N*,*N*′-Di(4-pyridyl)-1,6,7,12-tetrakis(4′-*tert*-butylphenoxy)perylene-3,4:9,10-tetracarboxylic acid bisimide [BPyPDI] (**16**) was prepared following reported procedures and used as the PDI-based oxidizing moiety.[35]

RuPcs form stable and rigid architectures through metal coordination of σ-donor, π-acceptor ligands such as pyridine.[21a,24,36] As aforementioned, the strongly ligating carbonyl ligand, occupying one of the two axial Ru(II) coordination sites, ensures exclusive coordination of the perylenediimide–bispyridyl ligand [BPyPDI] to the opposite Pc axial coordination site.[21a,19b,24,37]

Ruthenium complexes **1b**, **2b**, and **3b** were prepared in 78, 58 and 68% yield, respectively, by treating [BPyPDI] (**16**) with an excess of the corresponding ruthenium carbonyl phthalocyanine **5**, **9**, or **15**, in chloroform at room temperature. The reactions were monitored by ^{1}H NMR until neither starting PDI nor 1:1 Pc-PDI complexes were observed. Owing to the strength of the ruthenium–pyridyl coordination bond, **1b**, **2b**, and **3b** could be isolated by size exclusion chromatography and chemically characterized with standard techniques, namely ^{1}H and ^{13}C NMR, IR, and UV/vis spectroscopies.

^{1}H NMR spectra of **1b**, **2b**, and **3b** provide unequivocal evidence for the formation of the [Ru(CO)Pc]-[BPyPDI]-[Ru(CO)Pc] assemblies. Specifically, [BPyPDI] is located orthogonal to and between the two [Ru(CO)Pc] rings, so that it is influenced by the [Ru(CO)Pc] diamagnetic ring currents, falling in the shielding cone. As a matter of fact, all [BPyPDI] signals are shifted upfield and the extent of this effect depends on the distance between a given proton and the Pc core.

Figures 1, S51, and S52 represent comparative ^{1}H NMR spectra of non-coordinated and coordinated [BPyPDI]. The

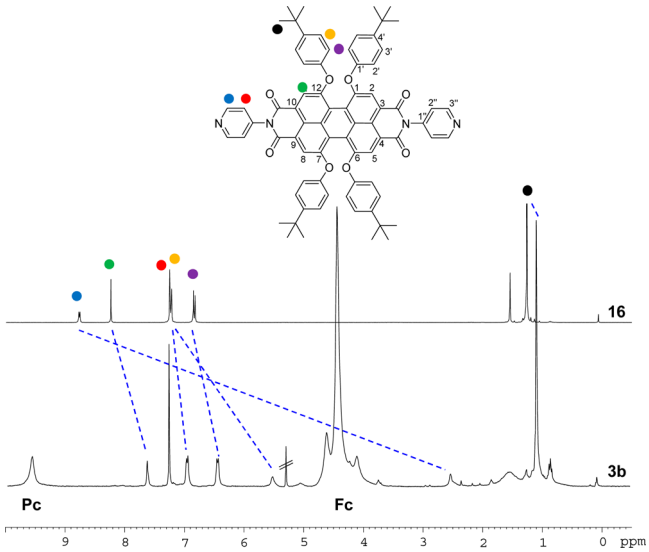

Figure 1. Comparative ^{1}H NMR spectra ($CDCl_3$) of [BPyPDI] (**16**) and [Ru(CO)Fc$_8$Pc]-[BPyPDI]-[Ru(CO)Fc$_8$Pc] (**3b**), showing the upfield shifts of PDI protons upon coordination.

shielding effect is particularly pronounced for the pyridyl substituents. Hereby, the H$^{3''}$ and H$^{5''}$ pyridyl protons display the strongest upfield shift appearing at δ = 2.08, 2.28, and 2.58 ppm for **1b**, **2b**, and **3b**, respectively, followed by H$^{2''}$ and H$^{6''}$, with values of 5.20, 5.31, and 5.54 ppm for **1b**, **2b**, and **3b**, respectively.

The most significant features of [Ru(CO)Pc]–[BPyPDI]–[Ru(CO)Pc] in IR spectroscopy are metal–carbonyl stretching bands at 1961, 1979, and 1967 cm^{-1}, in addition to two bands at 1710, 1681 (**1b**), 1712, 1683 (**2b**), and 1711, 1680 cm^{-1} (**3b**) corresponding to the PDI imido functions.

Assembly of Cart-Wheel Zn (II) Complexes 1a, 2a, and 3a. ^{1}H NMR Studies. The assembly of 2:1 ZnPc-PDI complexes **1a**, **2a**, and **3a** was investigated through titrations of [BPyPDI] (**16**) with ZnPcs **4**, **7**, and **12**.

In addition, 1:1 ZnPc-PDI model complexes were assembled using the monodentate [PyPDI] (**17**), which was prepared following a reported procedure,[14c] and used for coordination with ZnPcs **4**, **7**, and **12**. The Pc-PDI binding was monitored by ^{1}H NMR using a 6×10^{-3} M solution of **16** or **17** in $CDCl_3$ at 20 °C, and slowly adding the corresponding ZnPc. Titration

DOI: 10.1021/jacs.6b07432
J. Am. Chem. Soc. 2016, 138, 12963–12974

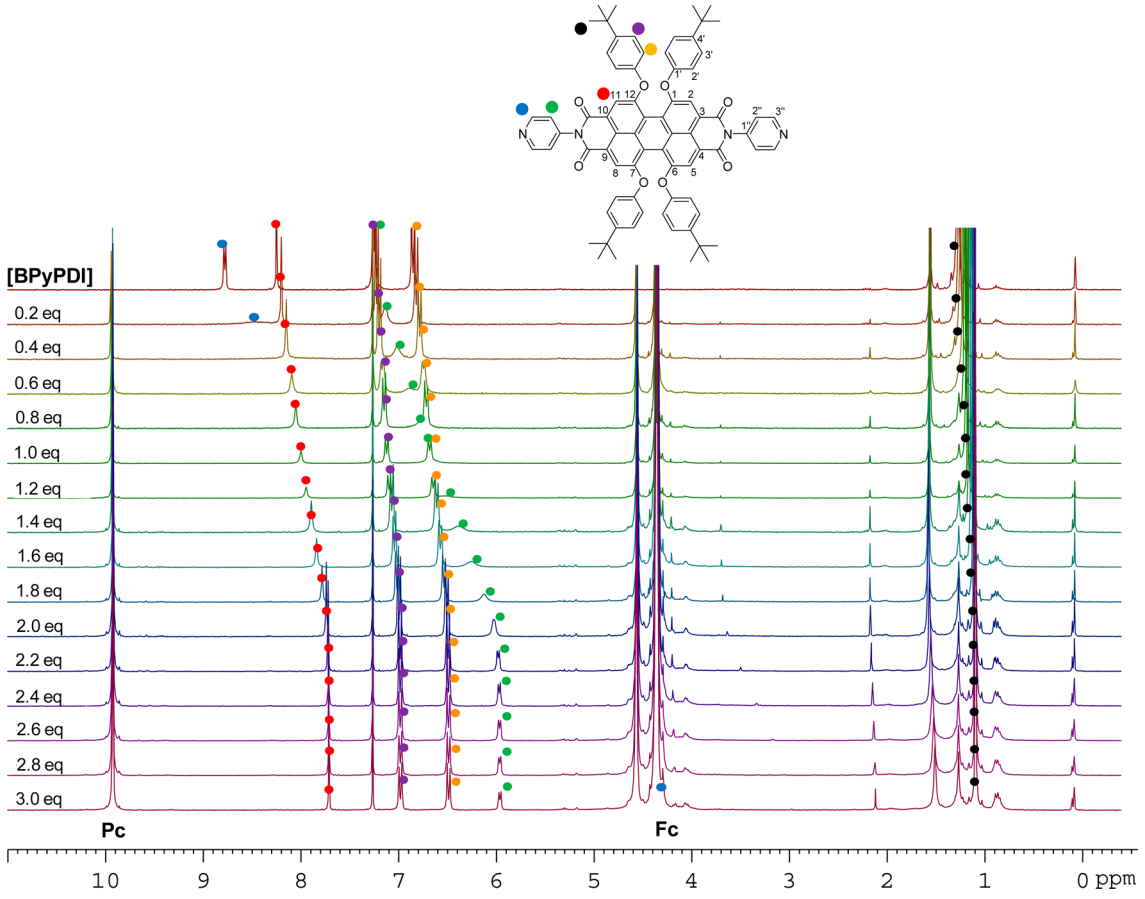

Figure 2. ^{1}H NMR titrations (300 MHz, 298 K) of [BPyPDI] (**16**) (6.0 mM) with [ZnFc$_8$Pc] (**12**) showing the change in chemical shifts ($\Delta\delta$) for [BPyPDI] in $CDCl_3$.

experiments under these conditions resulted in upfield shifts for the resonances of the PDI protons. As for the ruthenium complexes, this is due to the coordination of the pyridyl substituents of **16** and **17** (Chart S1 and Figures 2 and 3), resulting in an orthogonal disposition of the two chromophores, with the consequent shielding of the PDI protons by the Pc diatropic ring current.

Figures 2 and S53 represent the changes in the ^{1}H NMR spectra of [BPyPDI] (**16**) upon addition of ZnPcs **12** and **7**, respectively. The fact that we do not observe a mixture of signals corresponding to the non-coordinated, mono-coordinated, and di-coordinated species indicates that the relative exchange rate of the system at room temperature is fast at the time scale of the NMR experiment. Moreover, progressive exchange-broadening of pyridyl signals on the NMR time scale is observed upon titration until saturation at 2.2 equiv of ZnPcs (Figures 2 and S53). At the saturation point, the H$^{2''}$ and H$^{6''}$ protons sharpen, showing their original multiplicity and the highest upfield shift, appearing at δ = 5.50 and 6.00 ppm for **2a** and **3a**, respectively. The signals corresponding to the closest H$^{3''}$ and H$^{5''}$ pyridyl protons broaden and disappear. COSY-NMR of a 1:3 mixture of [BPyPDI] (**16**) and [ZnFc$_8$Pc] (**12**) (Figure S54), allows to determine a chemical shift of 4.3 ppm for these protons. There is a noticeable 1.7 ppm shielding of the H$^{3''}$ and H$^{5''}$ protons in the ruthenium complex **3b** (Figure 1) related to the corresponding signal in the zinc complex **3a** (Figure 2), reflecting the weaker and longer nature of the latter.

The titrations of the monodentate [PyPDI] (**17**) with ZnPcs **7** and **12** to afford complexes **18a** and **19a** are represented in Figure S55 and Figure 3, respectively. Now the saturation point appears around 1.4 equiv of added ZnPc, and the PDI signals undergo a slightly shorter upfield shift, when compared to the corresponding 2:1 complexes. For example, the pyridyl H$^{2''}$ and H$^{6''}$ protons (Figure S55, green dot) shift is $\Delta\delta \approx 1.3$ ppm in the 1:1 Pc-PDI complex **18a**, while the 2:1 complex **2a** displays a shift of $\Delta\delta \approx 1.7$ ppm upon coordination (Figure S53). This difference arises from the different number of orthogonal Pcs in the two complexes.

Next, the stoichiometry of the Zn complexes was corroborated by the mole ratio method.[38] Thus, inspection of the ^{1}H NMR data from the titration of [BPyPDI] (**16**) with ZnPcs in $CDCl_3$ by examination of the H$^{2''}$ and H$^{6''}$ binding isotherms show 1:2 equilibria (Figure 4), while the binding isotherms of H^2 and H^5 corresponding to the titration of [PyPDI] (**17**) with ZnPcs confirmed the expected 1:1 ZnPc-PDI ratio.

Finally, we used the data from the ^{1}H NMR titrations to calculate the association constants. The fitting of the NMR data was performed using two different software, namely *fittingprogram*[38a] and *HypNMR2008*.[39] Tables 1 and 2 summarize the results obtained after fitting the titration data of [PyPDIs] **16** and **17** with ZnPcs **7** and **12**, using the chemical shifts of H^2, H^{11} protons of PDI, in addition to H$^{2''}$ of the pyridine and the two H$^{2'}$ protons corresponding to the two magnetically different *tert*-butylphenoxy groups. The σ values in *HypNMR2008* show that the fitting is quite good. Besides, *fittingprogram* shows reasonable values of uncertainty by applying the global fitting (Table 1).[40]

DOI: 10.1021/jacs.6b07432
J. Am. Chem. Soc. 2016, 138, 12963−12974

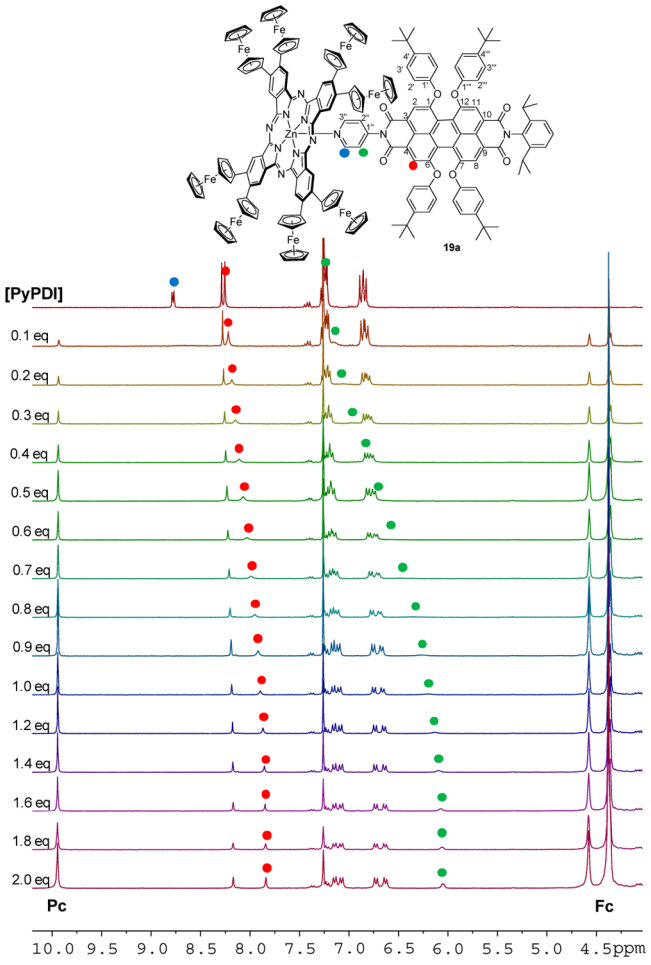

Figure 3. ^{1}H NMR titration (300 MHz, 298 K) of [PyPDI] (**17**) (6.0 mM) with [ZnFc$_8$Pc] (**12**) monitoring the formation of the 1:1 [PyPDI]:[ZnFc$_8$Pc] complex **19a**.

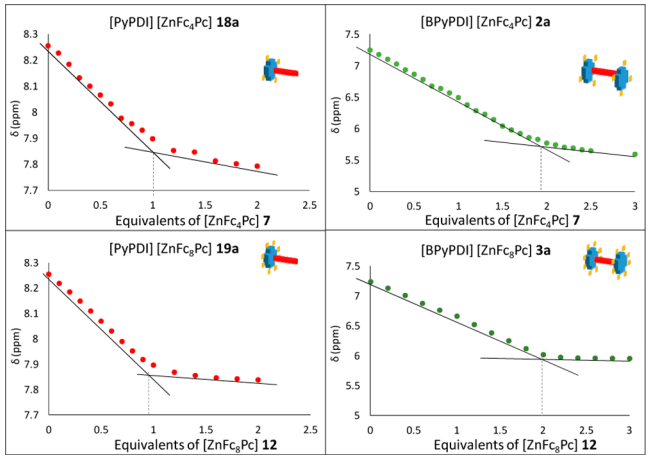

Figure 4. Plots of ^{1}H NMR titrations of [PyPDI] (**17**) and [BPyPDI] (**16**) with ZnPcs **7** and **12**, showing the changes in the chemical shifts of the H^2 and H^5 PDI protons (top left and bottom left), and the H$^{2''}$ and H$^{6''}$ pyridyl protons (top right and bottom right). The apparently linear portions at the beginning and the end of the curve are extrapolated to find a break point, corresponding to the ZnPc/PDI stoichiometric ratio.

Figure 5 shows the plots of ^{1}H NMR titrations with the changes in chemical shifts for each of the four protons of PDIs studied upon addition of ZnFc$_4$Pc (**7**) as analyzed by *HypNMR2008*. The calculated binding isotherms are in sound agreement with those determined in the experiments. Furthermore, comparison of the association constants for tetra- and octaferrocenyl systems (Table 1) reveals a higher binding constant (by 1 order of magnitude) for [PyPDI]·[ZnFc$_8$Pc] (**19a**) relative to [PyPDI]·[ZnFc$_4$Pc] (**18a**), with values of ~6.0 × 10^3 and 8.5 × 10^2 M^{-1}, respectively.

With respect to the 1:2 systems—i.e., coordination of [BPyPDI]—the values for k_2 were calculated using

Table 1. Calculated Binding Constants K_a for 18a and 19a from ^{1}H NMR Titration in CDCl$_3$ at 293 K of [PyPDI] (17) with [ZnFc$_4$Pc] (7) and [ZnFc$_8$Pc] (12)

	K_a/M^{-1} [a]	σ [a]	K_a/M^{-1} [b]
[PyPDI]·[ZnFc$_4$Pc] (**18a**)	852.5	0.0627	853 ± 29%
[PyPDI]·[ZnFc$_8$Pc] (**19a**)	5960	0.0764	6759 ± 40%

[a]Calculated with *HypNMR2008*, σ = standard deviation. [b]Calculated with *Fittingprogram* with expanded uncertainties at the 95% confidence intervals (%).

Table 2. Calculated Binding Constants K_1 and K_2 for 2a and 3a from ^{1}H NMR Titration in CDCl$_3$ at 293 K of [PyPDI] (17) with [ZnFc$_4$Pc] (7) and [ZnFc$_8$Pc] (12)

	K_1/M^{-1}	K_2/M^{-1}	σ
[BPyPDI]·[ZnFc$_4$Pc]$_2$ (**2a**)	1705	3969	0.07
[BPyPDI]·[ZnFc$_8$Pc]$_2$ (**3a**)	11921	32097	0.0843

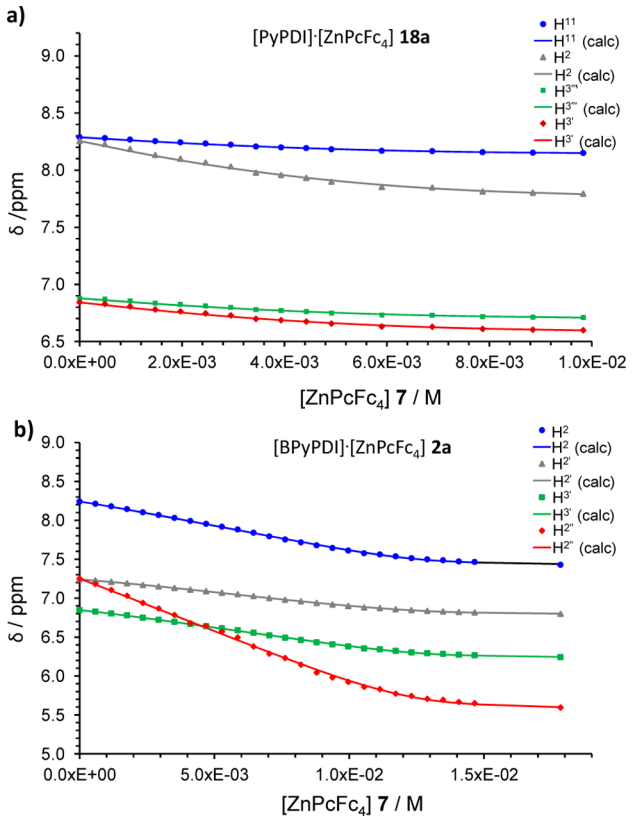

Figure 5. Plots of ^{1}H NMR titrations showing the change in chemical shifts after the addition of ZnPc$_4$Pc **7** for each of the (a) [PyPDI] (**17**) or (b) [BPyPDI] (**16**). The points represent the experimental changes on the chemical shifts and the lines the calculated points by *HypNMR2008*.

DOI: 10.1021/jacs.6b07432
J. Am. Chem. Soc. 2016, 138, 12963−12974

Table 3. Redox Potentials (in V) vs FcH/FcH$^+$ of ZnPcs 4, 7, and 12, RuPcs 5, 9, and 15, PDI 16, and Cart-Wheel Complexes 2b and 3b in DCM (0.1 M $TBAPF_6$) at Room Temperature Using a Glassy Carbon Electrode

complex	E_{red4}	E_{red3}	E_{red2}	E_{red1}	E_{ox1}	E_{ox2}	E_{ox3}	E_{ox4}
4				−1.47	0.10	0.83		
7				−1.61[a]	0.02	0.44		
12					−0.03	0.05	0.46[a]	0.94[a]
5		−1.59	−1.33[a]	−0.36[a]	0.21	0.49[a]	0.97	
9			−1.56[a]	−0.78[a]	0.04	0.59	1.06[a]	
15					−0.09	0.00	0.61[a]	
16			−1.24	−1.07	0.94	1.07[a]		
2b	−1.91	−1.51	−1.19	−1.06	0.03	0.54[a]		
3b	−2.00	−1.62	−1.20	−1.07	0.00	0.12[a]	0.64[a]	

[a]Irreversible.

HypNMR2008 and fixing k_1 to be the double the value found for the 1:1 systems (Table 2). The determined binding constants are in the range 10^3−10^4 M^{-1}. Again, octaferrocenyl complex [BPyPDI]·$[ZnFc_8Pc]_2$ (**3a**) exhibits 1 order of magnitude higher binding affinity related to tetraferrocenyl complex [BPyPDI]·$[ZnFc_4Pc]_2$ (**2a**). *Fittingprogram* was unable to produce a good fit when calculating 1:2 systems. For example, in the titration of [BPyPDI] (**16**) with $[ZnFc_8Pc]$ (**12**), values of k_1 = 3263 ± 183% M^{-1} and k_2 = 54 742 ± 132% M^{-1} were obtained.

Electrochemical Studies. Electrochemical experiments were conducted to investigate the influence of the ferrocene functionalization on the Pc units (Figures S56−S64). All of them display adsorption processes, similarly to what had been observed by Lever and Leznoff in related macrocycles.[29] Table 3 shows the reduction and oxidation potentials of ZnPcs **4**, **7**, and **12** and RuPcs **5**, **9**, and **15**, namely ferrocene- and *tert*-butyl-substituted Pcs. When compared to tetra-*tert*-butyl-phthalocyanines **4** and **5**, an additional oxidation, which is observed at +0.02 and +0.04 V in **7** and **9**, respectively, correlates to the attached ferrocenes.

In both cases, the first Pc-centered oxidation is shifted to higher potentials, that is, to +0.44 and +0.59 V. For **12** and **15**, the ferrocene oxidation splits due to the spatial proximity of two adjacent ferrocenes. The corresponding oxidations occur at −0.03/+0.05 V and −0.09/0.00 V, respectively. In both cases, the first Pc-related oxidation at either +0.46 or +0.61 V turns out to be irreversible. When lowering the temperature to 273 K for **7**, the ferrocene oxidation broadens remarkably and a multiple Gaussian fit reveals two subsequent oxidation processes at +0.01 and +0.06 V. From the latter we derive electronic communications of one ferrocene unit with another across the Pc (Figure 6).

The first oxidation and reduction potentials of cart-wheel complexes **2b** and **3b** show little variation with respect to those of the corresponding molecular units **9**, **15**, and **16**, reflecting the little communication between the Pc and PDI chromophores for this orthogonal conjugate in the ground state.

Photochemistry. *Steady State.* Absorption spectra of **16** and **17** in chlorobenzene show the typical PDI absorption features spanning from 400 to 650 nm with the most prominent maxima at 545 and 585 nm. Fluorescence maximizes at 613 nm with a shoulder around 670 nm. $[ZnBu_4Pc]$ (**4**) shows the typical ZnPc absorption features with a Q-band maximizing at 680 nm and fluorescence spanning from 685 to 800 nm. In the ferrocene containing Pcs **7** and **12** all absorption features are substantially red-shifted. The corresponding Q-band maxima appear at either 720 or 750 nm. Specifically, there

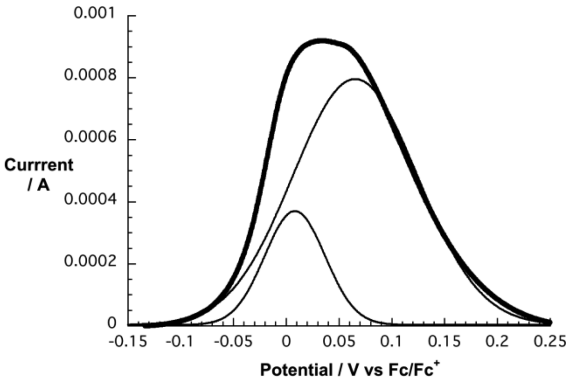

Figure 6. Square wave voltammogram of **7** (thick line) and corresponding Gaussian fit (thin lines) in DCM (0.1 M $TBAPF_6$) at 273 K using a glassy carbon electrode. Scan direction from −0.15 to +0.25 V. Potentials vs FcH/FcH$^+$.

is a 40 nm red shift of the Q-band on going from tetralkyl-substituted **4** to the tetraferrocene **7**.

Introduction of another four ferrocenes, to afford octasubstituted **12**, results in a 30 nm red shift of the Q-band. This observation suggests an 8−10 nm red shift of the Q-band for each ferrocene unit.

Furthermore, for **7** and **12** broad absorption features in the visible around 560 nm and weaker features at 860 and 910 nm, respectively, are observed (Figures S65 and S66). We assign these features to intervalent charge transfer (IVCT) between the Pcs and the peripheral ferrocenes. Neither **7**, nor **12** show any fluorescence.

When [BPyPDI] (**16**) or [PyPDI] (**17**) is added to a solution of $[ZnBu_4Pc]$ **4** in chlorobenzene (formation of complexes **1a** and **20**, Charts 1 and S1, respectively), no considerable ground-state interactions are observed. The absorption spectra resemble the superimposition of the PDI and ZnPc absorptions. Proof for complexation and electronic interactions came from fluorescence titrations. Upon addition of PDIs **16** or **17**, the ZnPc fluorescence is strongly quenched (Figure S70).

When $[ZnFc_4Pc]$ (**7**) and $[ZnFc_8Pc]$ (**12**) are treated similarly (formation of complexes **18a** and **19a**, respectively), the absorption spectra show intense ground-state interactions. Here, the ZnPc Soret band features are shifted bathochromically upon PDI addition. Additionally, the Q-band region is shifted hypsochromically (Figures 7a and S71).

When titrating the reverse direction, that is, adding Pcs **4**, **7**, or **12** to solutions of PDIs **16** and **17**, respectively, the absorption features are subject to a slight red shift. Importantly,

DOI: 10.1021/jacs.6b07432
J. Am. Chem. Soc. 2016, 138, 12963−12974

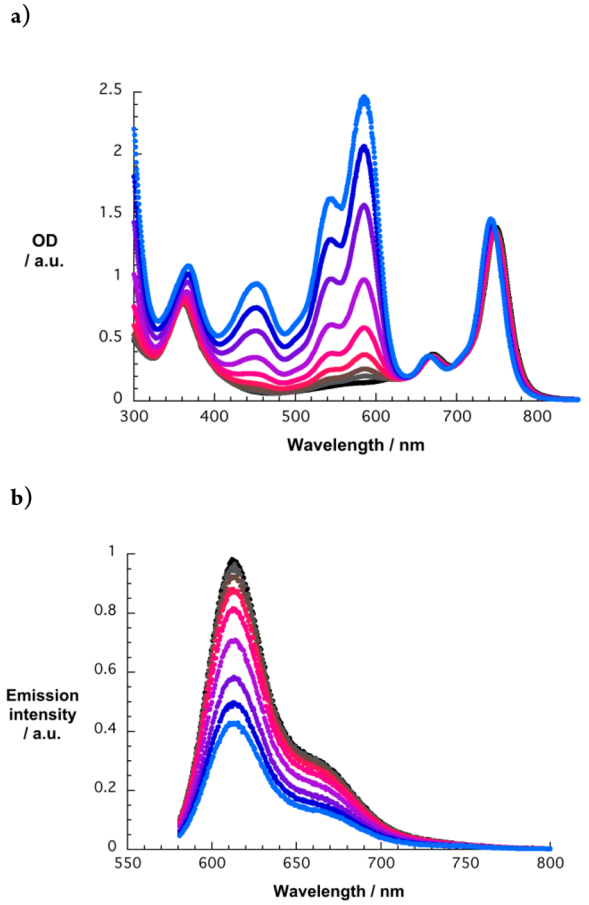

Figure 7. (a) Absorption spectrum of **12** (1.0×10^{-5} M) upon addition of different concentrations of **16** (0, 1.2×10^{-6}, 2.3×10^{-6}, 4.5×10^{-6}, 8.7×10^{-6}, 1.6×10^{-5}, 2.8×10^{-5}, 3.9×10^{-5}, and 5.0×10^{-5} M) in chlorobenzene. (b) Emission spectra (λ_{ex} = 570 nm) of **16** (2.0×10^{-7} M) upon addition of different concentrations of **12** (0, 2.8×10^{-7}, 5.7×10^{-7}, 1.1×10^{-6}, 2.1×10^{-6}, 4.0×10^{-6}, 7.0×10^{-6}, 9.7×10^{-6}, and 1.2×10^{-5} M) in chlorobenzene.

the PDI fluorescence is strongly quenched in all cases (Figures 7b and S67–S69).

Absorption spectra of Ru(II)Pcs **5**, **9**, and **15** show the typical Soret- and Q-band features. In ferrocene containing **9** and **15**, these features are, again, dramatically red-shifted when compared to **5** lacking any ferrocene (Figures 8, S72, S75, and S76). Furthermore, the functionalization with ferrocene leads to the formation of a broad absorption band in the visible region from 350 to 600 nm, making both panchromatic light absorbers from below 300 nm to above 850 nm.

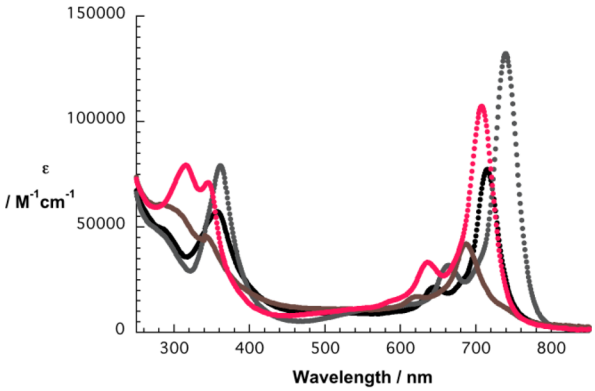

Figure 8. UV/vis spectra of $ZnFc_4Pc$ **7** (black), **12** (gray), **9** (brown), and **15** (pink) in chloroform.

When compared to the monomeric building blocks, RuPc-PDI 2:1 complexes **1b** (Figure S72), **2b** (Figure S75), and **3b** (Figure S76) show the following changes in the absorption spectra: (i) a red shift of the PDI-centered features and (ii) a blue shift in the Pc Q-band region. These changes are attributed to the strong coordinative binding and the resulting ground-state interactions, i.e., a shift of electron density from the electron-donating Pc to the electron-accepting PDI.

Upon 650 nm photoexcitation, **5** shows typical fluorescence which is dramatically quenched in **1b** (Figure S74). Ferrocene-containing Pcs **9** and **15** fail to show any appreciable fluorescence. This finding is rationalized by the presence of the ferrocenes. The PDI-centered fluorescence is dramatically quenched in **1b**, **2b**, and **3b** (Figures 9, S73, and S77). From the aforementioned observations, we conclude that PDI and RuPc strongly interact in **1b**, **2b**, and **3b** in the ground as well as in the excited state.

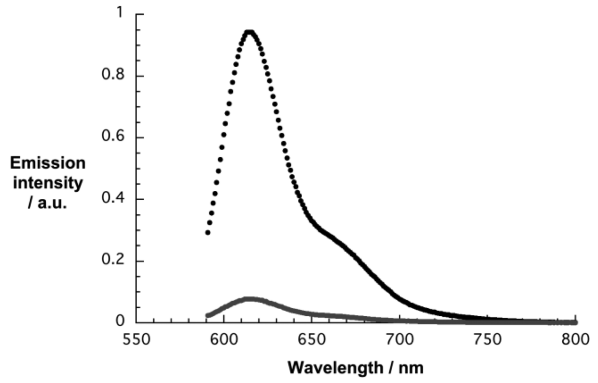

Figure 9. Emission spectra of 1.0×10^{-6} M solutions of **16** (black) and **2b** (gray) upon 570 nm photoexcitation in chlorobenzene.

Taking the changes in terms of fluorescence quenching into account when titrating PDIs **16** and **17** with RuPcs **9** and **15** (formation of complexes **2b**, **3b**, **18b**, and **19b**, Charts 1 and S1, respectively), nonlinear curve fitting allowed for determination of the association constants for the 1:1 and 2:1 ruthenium complexes using the ReactLab EQUILIBRIA software. The corresponding constants are fairly high with K_a values of around 10^{-6}–10^{-7} M^{-1} (Table 4).

Transient Absorption. To shed light onto the excited-state interactions, transient absorption measurements were conducted. [$ZnBu_4Pc$] (**4**) shows after conclusion of the 150 fs laser pulse (λ_{ex} = 676 nm) the typical transient absorption features of ZnPc in chlorobenzene (Figure S78). In particular, transient maxima at 454, 599, 637, and 829 nm, which are

Table 4. Association Constants [M^{-1}] of RuPcs 9 and 15 with PDIs 16 and 17 Derived from Fluorescence Quenching Titrations in Chlorobenzene

	K_1/M^{-1}	K_2/M^{-1}
[PyPDI]·[$RuFc_4Pc$] (**18b**)	$(4.11 \pm 0.04) \times 10^6$	
[PyPDI]·[$RuFc_8Pc$] (**19b**)	$(3.40 \pm 0.03) \times 10^6$	
[PyPDI]·[$RuFc_4Pc]_2$ (**2b**)	$(1.91 \pm 0.03) \times 10^6$	$(1.47 \pm 0.03) \times 10^7$
[PyPDI]·[$RuFc_8Pc]_2$ (**3b**)	$(7.23 \pm 0.11) \times 10^5$	$(2.58 \pm 0.05) \times 10^7$

DOI: 10.1021/jacs.6b07432
J. Am. Chem. Soc. 2016, 138, 12963–12974

accompanied by ground-state bleaching around 616, 633, and 684 nm corroborate the formation of the ZnPc singlet excited state. These features deactivate via intersystem crossing within approximately 3 ns to the lower lying triplet excited state exhibiting a transient maximum at 494 nm. Nanosecond transient absorption measurements assisted in determining a lifetime of the triplet excited state of 22.5 μs. After photoexcitation, [$ZnFc_4Pc$] (**7**) shows similar transients including maxima at 477, 622, and 853 nm and ground-state bleaching around 657 and 724 nm (Figure S79). In contrast to **4**, these singlet excited-state features deactivate within 3.6 ps to yield the triplet excited state, which is identified by transient maxima at 490, 524, and around 1100 nm. The deactivation to the ground state takes place within 3.0 ns after excitation. A similar picture is gathered when exciting [$ZnFc_8Pc$] (**12**) (Figure S80). Here, the singlet excited-state features at 506, 648, 700, and 820 nm as well as ground-state bleach at 674 and 750 nm deactivate within 4.4 ps to the triplet excited state. The triplet deactivates within 4.5 ns to the ground state. This very fast intersystem crossing and the subsequent deactivation to the ground state is rationalized by the presence of either four or eight ferrocenes in **7** and **12**, respectively. This observation is well in line with the absence of any detectable fluorescence.

Instantaneously after conclusion of the laser pulse, [$RuBu_4Pc$] (**5**) shows the typical transient features of the singlet excited state of RuPc in chlorobenzene, that is, transient absorptions maximizing at 545, 586, 918, and around 1200 nm, as well as ground-state bleaching minimizing at 634 and 677 nm (Figure S81). Within 9 ps, these singlet features deactivate to the RuPc triplet excited state identified by transient maxima at 514, 543, 664, and 952 nm. These long-lived features exceed the limits of our femtosecond setup. Nanosecond transient absorption measurements revealed a lifetime of 6.9 μs for the triplet excited state of **5**. When exciting [$RuFc_4Pc$] (**9**), RuPc triplet excited-state features appear within the instrument response time (<1 ps, Figure S82). This acceleration is attributed to the presence of the four ferrocenes on the RuPc periphery. The RuPc triplet excited state of **9** deactivates within 209 ns to the electronic ground state. [$RuFc_8Pc$] (**15**) shows a similar behavior with a shorter triplet excited-state lifetime of 1.6 ns (Figure S83).

Upon 568 nm photoexcitation, **16** and **17** show the typical transient absorption features of PDIs in the form of maxima around 710, 970, and 1045 nm as well as minima at 460, 544, 598, and 670 nm (Figures S84 and S85). These features deactivate to the ground state within 5.8 ns. The kinetic data are presented in Table 5.

When **20** is excited at 676 nm, where only ZnPc absorbs, initially ZnPc singlet excited-state features are observed. Within 53 ps, these features are replaced by the typical transient absorption features of the ZnPc radical cation, that is, a 846 nm maximum, and the PDI radical anion, that is, 792, 987, and 1093 nm maxima, arise (Figure S86), respectively.[14c,21e,22d,41] The correspondingly formed charge-separated state $ZnPc^{\bullet+}$-$PDI^{\bullet-}$ recombines within 2050 ps to the triplet manifold of the ZnPc, which subsequently deactivates to the ground state. In **1a** the observations are very similar (Figure S87), and the kinetic data are presented in Table 6. Excitation of **20** and **1a** at 568 nm exclusively yields the singlet excited-state features of PDI (Figures S88 and S89). Subsequent electron transfer from the ground-state ZnPc to the excited-state PDI leads to the formation of the charge-separated states within 57 and 51 ps, respectively. When **2a**, **18a**, **3a**, and **19a** are excited at 676 nm, only ZnPc-centered transients are observed (Figures S90–S93).

The singlet excited state deactivates rapidly to the triplet excited state, as seen for **7** and **12**, which then transforms into the ZnPc ground state. We attribute this lack of electronic interaction between ZnPc and PDI to the very fast deactivation of the ZnPc singlet excited state induced by the presence of the ferrocene units.

Upon 568 nm photoexcitation of **2a**, **18a**, **3a**, and **19a**, the singlet excited-state features of PDI are visible. Within about 2–5 ps these features fade away, while the typical transient features of the ZnPc triplet excited state evolve. A likely rationale for this observation is a fast energy transfer from the excited state PDI to ZnPc, populating the ZnPc singlet excited state (see Table 7). As intersystem crossing in **7** and **12** is, at about 4 ps, very fast, the typical singlet excited-state transients of ZnPc are masked. Only the triplet excited-state features are discernible, and these subsequently deactivate to the electronic

Table 5. Singlet (S) and Triplet (T) Excited-State Lifetimes of ZnPcs 4, 7, and 12, RuPcs 5, 9, and 15, and PDIs 16 and 17 upon 676 nm (Pc) and 568 nm (PDI) Photoexcitation in Chlorobenzene

complex	τ (^{1}*S)/ps	τ (^{3}*T)/ns
4	2820	22500
7	3.6	3.0
12	4.4	4.5
17	5795	
16	5753	
5	9	6900
9	<1	209
15	<1	1.6

Table 7. Rate Constants for Energy Transfer from PDI to ZnPc upon Photoexcitation (λ_{ex} = 568 nm) in Chlorobenzene

	k_{EnT}/s^{-1}
18a	2.1×10^{11}
2a	4.5×10^{11}
19a	2.6×10^{11}
3a	2.6×10^{11}

Table 6. Rate Constants for Charge Separation (CS) and Charge Recombination (CR) and Corresponding Lifetimes of the Charge-Separated States (CSS) $ZnPc^{\bullet+}$-$PDI^{\bullet-}$ upon 676 and 568 nm Photoexcitation in Chlorobenzene

	λ_{ex} = 676 nm			λ_{ex} = 568 nm		
	CS/s^{-1}	CR/s^{-1}	τ(CSS)/ps	CS/s^{-1}	CR/s^{-1}	τ(CSS)/ps
20	1.9×10^{10}	4.9×10^{8}	2050	1.7×10^{10}	4.3×10^{8}	2333
1a	2.1×10^{10}	6.2×10^{8}	1613	2.0×10^{10}	6.0×10^{8}	1663

DOI: 10.1021/jacs.6b07432
J. Am. Chem. Soc. 2016, 138, 12963–12974

Table 8. Rate Constants for Charge Separation (CS) and Charge Recombination (CR) and Corresponding Lifetimes of the Charge-Separated States (CSS) $RuPc^{\bullet+}$-$PDI^{\bullet-}$ upon 676 and 568 nm Photoexcitation in Chlorobenzene and Anisole

	chlorobenzene			anisole			benzonitrile		
	CS/s^{-1}	CR/s^{-1}	τ(CSS)/ps	CS/s^{-1}	CR/s^{-1}	τ(CSS)/ps	CS/s^{-1}	CR/s^{-1}	τ(CSS)/ps
1b (λ_{ex} = 676 nm)	2.0×10^{11}	3.1×10^{6}	320000						
1b (λ_{ex} = 568 nm)	1.2×10^{11}	3.0×10^{6}	331000	2.0×10^{11}	2.4×10^{6}	417000	3.3×10^{10}	3.9×10^{6}	259300
2b	7.6×10^{11}	4.3×10^{8}	2338	8.3×10^{11}	5.0×10^{8}	2031	4.4×10^{10}	2.8×10^{8}	3606
3b	1.0×10^{12}	8.2×10^{8}	1225	6.7×10^{11}	7.5×10^{8}	1340	8.3×10^{10}	2.3×10^{8}	4315

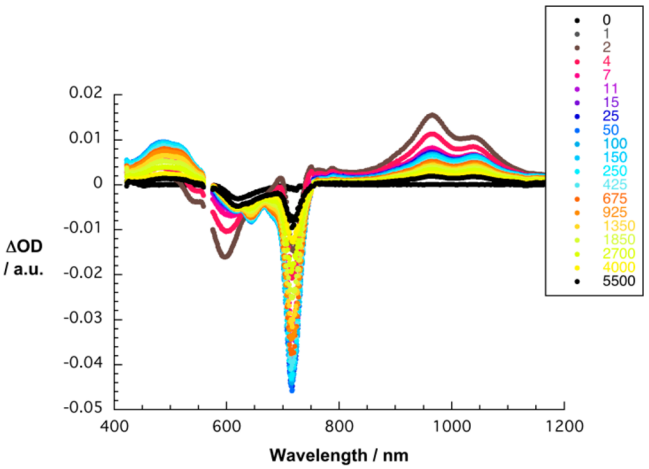

Figure 10. Femtosecond transient absorption spectra of **7**·**16** (2:1, ~10^{-5} M) in argon-saturated chlorobenzene upon 568 nm photoexcitation with time delays between 1 and 5500 ps, indicating the energy transfer from PDI to ZnPc at room temperature.

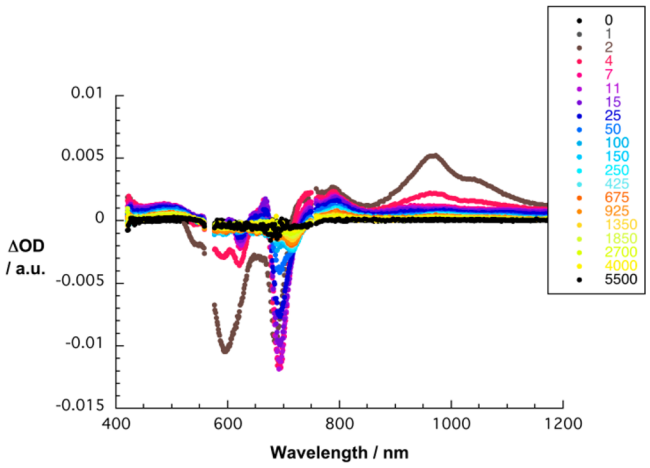

Figure 11. Femtosecond transient absorption spectra of **2b** (~10^{-5} M) in argon-saturated anisole upon 568 nm photoexcitation with time delays between 1 and 5500 ps, indicating charge separation and recombination at room temperature.

ground state within several nanoseconds (Figures 10 and S94–S96).

Upon 676 nm photoexcitation of **1b** in chlorobenzene (Table 8), the RuPc singlet excited-state features are seen to be deactivated within 5 ps and to transform into new transient features that were not detected in **5** and **16**. In this particular case, the new transient maximizing around 730 nm resembles what has been described as the radical cation of RuPc,[21a,42] whereas maxima at 795, 995, and 1100 nm corroborate the formation of the PDI anion (Figure S97). All of these features decay within 320 ns to the triplet excited state of RuPc.

When **2b** and **3b** were excited at 676 nm (Table 8), no evidence for any electron transfer was gathered. Any electronic interactions between RuPc in the excited state and the PDI in the ground state is hindered by the fast singlet excited-state deactivation induced by the ferrocene units in **2b** and **3b** (Figures S98 and S99). In light of the matter, we turned to 568 nm excitation (Table 8). In this particular case, PDI is exclusively excited, and hence the immediate influence of the ferrocenes on the excited state is minimized. As a matter of fact, for **1b** in chlorobenzene a 9 ps deactivation of the PDI singlet excited state at, for example, 980 nm, goes hand in hand with the growth of the radical ion species' bands. A transient at 730 nm reflects the generation of the RuPc cation, transients at 795, 995, and 1100 nm the PDI anion (Figure S100). For **2b** and **3b**, charge separation is even faster with ca. 1 ps. The charge recombination takes place within 2.3 and 1.2 ns, for **2b** and **3b**, respectively, and yields the RuPc triplet excited state. In less polar anisole, similar observations with comparable rates for charge separation and recombination were made (Figures 11, S103, and S104). In more polar benzonitrile, charge separation is decelerated by approximately 1 order of magnitude, while charge recombination occurs with comparable rates (Figures S105–S107).

CONCLUSIONS

The direct attachment of four or eight ferrocenes to the peripheral positions of ZnPcs and RuPcs evokes significant alterations in the electronic features. These changes are reflected by large bathochromic shifts of the Q-band absorptions with 8–10 nm per ferrocene and low oxidation potentials arising from the ferrocene units. When these tetra- and octaferrocenylphthalocyanines are integrated into cart-wheel-shaped Pc-PDI electron donor–acceptor systems, RuPcs enable the generation of $Pc^{+\bullet}$-$PDI^{-\bullet}$ radical ion pair states upon PDI photoexcitation. Rather than stabilizing the generated radical ion pair states, the presence of peripheral ferrocenes accelerates the charge recombination process. In the corresponding ZnPcs, energy transfer from PDI to ZnPc is observed, ultimately yielding the ZnPc triplet excited state, which then deactivates to the ground state.

ASSOCIATED CONTENT

Supporting Information

The Supporting Information is available free of charge on the ACS Publications website at DOI: 10.1021/jacs.6b07432.

Structures of all the synthesized systems, experimental procedures, and full chemical and photophysical characterization, including Chart S1, Schemes S1–S3, and Figures S1–S107 (PDF)

DOI: 10.1021/jacs.6b07432
J. Am. Chem. Soc. 2016, 138, 12963–12974

AUTHOR INFORMATION

Corresponding Authors

*salome.rodriguez@uam.es
*dirk.guldi@chemie.uni-erlangen.de
*tomas.torres@uam.es

Notes

The authors declare no competing financial interest.

ACKNOWLEDGMENTS

Financial support from Solar Technologies Go Hybrid (Sol-Tech), SFB953, Comunidad de Madrid, Spain (S2013/MIT-2841, FOTOCARBON), and Spanish MICINN (CTQ2014-52869-P) is acknowledged. J.F.-A. acknowledges Spanish MICINN for his F.P.U. fellowship.

REFERENCES

(1) (a) Nocera, D. G. *Acc. Chem. Res.* **2012**, *45*, 767−776. (b) Schreier, M.; Curvat, L.; Giordano, F.; Steier, L.; Abate, A.; Zakeeruddin, S. M.; Luo, J.; Mayer, M. T.; Grätzel, M. *Nat. Commun.* **2015**, *6*, 7326. (c) Duan, L.; Wang, L.; Li, F.; Li, F.; Sun, L. *Acc. Chem. Res.* **2015**, *48*, 2084−2096. (d) Bard, A. J.; Fox, M. A. *Acc. Chem. Res.* **1995**, *28*, 141−145. (e) Gust, D.; Moore, T. A.; Moore, A. L. *Acc. Chem. Res.* **2009**, *42*, 1890−1898.

(2) (a) Balzani, V.; Credi, A.; Venturi, M. *ChemSusChem* **2008**, *1*, 26−58. (b) Eisenberg, R.; Nocera, D. G. *Inorg. Chem.* **2005**, *44*, 6799−6801 and references therein. (c) Arakawa, H.; Aresta, M.; Armor, J. N.; Barteau, M. A.; Beckman, E. J.; Bell, A. T.; Bercaw, J. E.; Creutz, C.; Dinjus, E.; Dixon, D. A.; Domen, K.; DuBois, D. L.; Eckert, J.; Fujita, E.; Gibson, D. H.; Goddard, W. A.; Goodman, D. W.; Keller, J.; Kubas, G. J.; Kung, H. H.; Lyons, J. E.; Manzer, L. E.; Marks, T. J.; Morokuma, K.; Nicholas, K. M.; Periana, R.; Que, L.; Rostrup-Nielson, J.; Sachtler, W. M. H.; Schmidt, L. D.; Sen, A.; Somorjai, G. A.; Stair, P. C.; Stults, B. R.; Tumas, W. *Chem. Rev.* **2001**, *101*, 953−996. (d) Wasielewski, M. R. *Chem. Rev.* **1992**, *92*, 435−461. (e) Kim, D.; Sakimoto, K. K.; Hong, D.; Yang, P. *Angew. Chem., Int. Ed.* **2015**, *54*, 3259−3266.

(3) (a) Concepcion, J. J.; House, R. L.; Papanikolas, J. M.; Meyer, T. J. *Proc. Natl. Acad. Sci. U. S. A.* **2012**, *109*, 15560−15564. (b) Alstrum-Acevedo, J. H.; Brennaman, M. K.; Meyer, T. J. *Inorg. Chem.* **2005**, *44*, 6802−6827.

(4) (a) Wasielewski, M. R. *Acc. Chem. Res.* **2009**, *42*, 1910−1921. (b) Wasielewski, M. R. *Chem. Rev.* **1992**, *92*, 435−461. (c) Sun, L.; Hammarstrom, L.; Akermark, B.; Styring, S. *Chem. Soc. Rev.* **2001**, *30*, 36−49. (d) KC, C. B.; D'Souza, F. *Coord. Chem. Rev.* **2016**, *322*, 104−141.

(5) (a) Balzani, V.; Moggi, L.; Scandola, F. Towards a Supramolecular Photochemistry: Assembly of Molecular Components to Obtain Photochemical Molecular Devices. In *Supramolecular Photochemistry*; Balzani, V., Ed.; D. Reidel Publishing Co.: Dordrecht, Holland, 1987; pp 1−28. (b) *Electron Transfer in Chemistry*; Balzani, V., Ed.; Wiley-VCH: Weinheim, Germany, 2001.

(6) (a) Speiser, S. *Chem. Rev.* **1996**, *96*, 1953−1976. (b) Fukuzumi, S.; Ohkubo, K.; Suenobu, T. *Acc. Chem. Res.* **2014**, *47*, 1455−1464. (c) Castellanos, S.; Vieira, A. A.; Illescas, B. M.; Sacchetti, V.; Schubert, C.; Moreno, J.; Guldi, D. M.; Hecht, S.; Martin, N. *Angew. Chem., Int. Ed.* **2013**, *52*, 13985−13990. (d) Wijesinghe, C.; El-Khouly, M. E. A.; Zandler, M. E.; Fukuzumi, S.; D'Souza, F. *Chem. - Eur. J.* **2013**, *19*, 9629−9638. (e) Shibano, Y.; Umeyama, T.; Matano, Y.; Tkachenko, N. V.; Lemmetyinen, H.; Imahori, H. *Org. Lett.* **2006**, *8*, 4425−4428. (f) Pillai, S.; Ravensbergen, J.; Antoniuk-Pablant, A.; Sherman, B. D.; van Grondelle, R.; Frese, R. N.; Moore, T. A.; Gust, D.; Moore, A. L.; Kennis, J. T. M. *Phys. Chem. Chem. Phys.* **2013**, *15*, 4775−4784.

(7) (a) O'Regan, B.; Grätzel, M. *Nature* **1991**, *353*, 737. (b) Grätzel, M. *Inorg. Chem.* **2005**, *44*, 6841−6851. (c) Meyer, G. J. *Inorg. Chem.* **2005**, *44*, 6852−6854. (d) Imahori, H.; Norieda, H.; Yamada, H.; Nishimura, Y.; Yamazaki, I.; Sakata, Y.; Fukuzumi, S. *J. Am. Chem. Soc.* **2001**, *123*, 100−110. (e) Li, L.-L.; Diau, E. W.-G. *Chem. Soc. Rev.* **2013**, *42*, 291−304.

(8) (a) Tebo, A.; Herrero, C.; Aukauloo, A. Porphyrins and metalloporphyrins as components in artificial photosynthesis research. In *Handbook of Porphyrin Science*; Kadish, K. M., Smith, K. M., Guilard, R., Eds.; World Scientific Publishing Co.: Singapore, 2014; Vol. *34*, pp 195−237. (b) Nagata, T. *Res. Chem. Intermed.* **2014**, *40*, 3183−3198. (c) Perchanova, M.; Kurreck, H.; Berg, A. *J. Phys. Chem. A* **2015**, *119*, 8117−8124. (d) Melomedov, J.; Ochsmann, J. R.; Meister, M.; Laquai, F.; Heinze, K. *Eur. J. Inorg. Chem.* **2014**, *2014*, 1984−2001.

(9) (a) Imahori, H.; Yamada, H.; Guldi, D. M.; Endo, Y.; Shimomura, A.; Kundu, S.; Yamada, K.; Okada, T.; Sakata, Y.; Fukuzumi, S. *Angew. Chem., Int. Ed.* **2002**, *41*, 2344−2347. (b) Balzani, V.; Credi, A.; Venturi, M. Photoinduced Charge Separation and Solar Energy Conversion. In *Molecular Devices and Machines: A Journey into the Nanoworld*; Balzani, V., Credi, A., Venturi, M., Eds.; Wiley-VCH: Weinheim, Germany, 2003; pp 132−173. (c) Harriman, A. *Chem. Commun.* **2015**, *51*, 11745−11756. (d) Bandi, V.; D'Souza, F. P.; Gobeze, H. B.; D'Souza, F. *Chem. - Eur. J.* **2015**, *21*, 2669−2679.

(10) *The Porphyrin Handbook*; Kadish, K. M., Smith, K. M., Guilard, R., Eds.; Academic Press: San Diego, CA, 2003; Vols. *15*−*20*.

(11) Rio, Y.; Rodríguez-Morgade, M. S.; Torres, T. *Org. Biomol. Chem.* **2008**, *6*, 1877−1894.

(12) (a) Hasobe, T. Supramolecular assemblies of porphyrin and phthalocyanine derivatives for solar energy conversion and molecular electronics. In *Handbook of Porphyrin Science*; Kadish, K. M., Smith, K. M., Guilard, R., Eds.; World Scientific Publishing Co.: Singapore, 2014; Vol. *34*, pp 147−194. (b) Fukuzumi, S. Artificial photosynthetic systems composed of porphyrins and phthalocyanines. In *Handbook of Porphyrin Science*; Kadish, K. M., Smith, K. M., Guilard, R., Eds.; World Scientific Publishing Co.: Singapore, 2010; Vol. *10*, pp 183−243. (c) de la Escosura, A.; Trukhina, O.; Torres, T. *Struct. Bonding (Berlin, Ger.)* **2013**, *159*, 145−191. (d) Bottari, G.; de la Torre, G.; Torres, T. *Acc. Chem. Res.* **2015**, *48*, 900−910.

(13) (a) McKeown, N. B. *Sci. Synth.* **2004**, *17*, 1237−1368. (b) Li, R.; Zhang, X.; Zhu, P.; Ng, D. K. P.; Kobayashi, N.; Jiang, J. *Inorg. Chem.* **2006**, *45*, 2327−2334. (c) Guldi, D. M.; Gouloumis, A.; Vázquez, P.; Torres, T. *Chem. Commun.* **2002**, 2056−2057. (d) Martínez-Díaz, M. V.; Fender, N. S.; Rodríguez-Morgade, M. S.; Gómez-López, M.; Diederich, F.; Echegoyen, L.; Stoddart, J. F.; Torres, T. *J. Mater. Chem.* **2002**, *12*, 2095−2099. (e) Li, X.; Sinks, L. E.; Rybtchinski, B.; Wasielewski, M. R. *J. Am. Chem. Soc.* **2004**, *126*, 10810−10811. (f) Langmar, O.; Ganivet, C. R.; Lennert, A.; Costa, R. D.; de la Torre, G.; Torres, T.; Guldi, D. M. *Angew. Chem., Int. Ed.* **2015**, *54*, 7688−7692. (g) Wibmer, L.; Lourenco, L. M. O.; Roth, A.; Katsukis, G.; Neves, M. G. P. M. S.; Cavaleiro, J. A. S.; Tome, J. P. C.; Torres, T.; Guldi, D. M. *Nanoscale* **2015**, *7*, 5674−5682.

(14) See, for example: (a) Miller, M. A.; Lammi, R. K.; Prathapan, S.; Holten, D.; Lindsey, J. S. *J. Org. Chem.* **2000**, *65*, 6634−6649. (b) Lee, C.; Guo, J.; Chen, L. X.; Mandal, B. K. *J. Org. Chem.* **2008**, *73*, 8219−8227. (c) Lederer, M.; Hahn, U.; Fernandez-Ariza, J.; Trukhina, O.; Rodriguez-Morgade, M. S.; Dammann, C.; Drewello, T.; Torres, T.; Guldi, D. M. *Chem. - Eur. J.* **2015**, *21*, 5916−5925. (d) González-Rodríguez, D.; Claessens, C. G.; Torres, T.; Liu, S.; Echegoyen, L.; Vila, N.; Nonell, S. *Chem. - Eur. J.* **2005**, *11*, 3881−3893. (e) Bottari, G.; de la Torre, G.; Torres, T. *Acc. Chem. Res.* **2015**, *48*, 900−910.

(15) Bottari, G.; de la Torre, G.; Guldi, D. M.; Torres, T. *Chem. Rev.* **2010**, *110*, 6768−6816.

(16) (a) Guldi, D. M.; Zilbermann, I.; Gouloumis, A.; Vázquez, P.; Torres, T. *J. Phys. Chem. B* **2004**, *108*, 18485−18494. (b) Guldi, D. M.; Gouloumis, A.; Vázquez, P.; Torres, T.; Georgakilas, V.; Prato, M. *J. Am. Chem. Soc.* **2005**, *127*, 5811−5813. (c) Gouloumis, A.; de la Escosura, A.; Vazquez, P.; Torres, T.; Kahnt, A.; Guldi, D. M.; Neugebauer, H.; Winder, C.; Drees, M.; Sariciftci, N. S. *Org. Lett.* **2006**, *8*, 5187−5190. (d) Isosomppi, M.; Tkachenko, N. V.; Efimov, A.; Vahasalo, H.; Jukola, J.; Vainiotalo, P.; Lemmetyinen, H. *Chem. Phys. Lett.* **2006**, *430*, 36−40. (e) Kahnt, A.; Guldi, D. M.; de la Escosura, A.; Martínez-Díaz, M. V.; Torres, T. *J. Mater. Chem.* **2008**, *18*, 77−82.

DOI: 10.1021/jacs.6b07432
J. Am. Chem. Soc. 2016, 138, 12963−12974

(17) (a) Fukuzumi, S.; Honda, T.; Ohkubo, K.; Kojima, T. *Dalton Trans.* **2009**, 3880−3889. (b) Linssen, T. G.; Durr, K.; Hanack, M.; Hirsch, A. *J. Chem. Soc., Chem. Commun.* **1995**, 103−104. (c) Quintiliani, M.; Kahnt, A.; Wölfle, T.; Hieringer, W.; Vázquez, P.; Görling, A.; Guldi, D. M.; Torres, T. *Chem. - Eur. J.* **2008**, *14*, 3765−3775. (d) El-Khouly, M. E.; Kang, E. S.; Kay, K.-Y.; Choi, C. S.; Aaraki, Y.; Ito, O. *Chem. - Eur. J.* **2007**, *13*, 2854−2863. (e) Martin-Gomis, L.; Ohkubo, K.; Fernandez-Lazaro, F.; Fukuzumi, S.; Sastre-Santos, A. *Org. Lett.* **2007**, *9*, 3441−3444.

(18) (a) de la Escosura, A.; Martinez-Diaz, M. V.; Guldi, D. M.; Torres, T. *J. Am. Chem. Soc.* **2006**, *128*, 4112−4118. (b) D'Souza, F.; Maligaspe, E.; Ohkubo, K.; Zandler, M. E.; Subbaiyan, N. K.; Fukuzumi, S. *J. Am. Chem. Soc.* **2009**, *131*, 8787−8797. (c) Martínez-Díaz, M. V.; Fender, N. S.; Rodríguez-Morgade, M. S.; Gómez-López, M.; Diederich, F.; Echegoyen, L.; Stoddart, J. F.; Torres, T. *J. Mater. Chem.* **2002**, *12*, 2095−2099. (d) Chen, Y.; El-Khouly, M. E.; Sasaki, M.; Araki, Y.; Ito, O. *Org. Lett.* **2005**, *7*, 1613−1616.

(19) (a) Ballesteros, B.; de la Torre, G.; Torres, T.; Hug, G. L.; Rahman, G. M. A.; Guldi, D. M. *Tetrahedron* **2006**, *62*, 2097−2101. (b) Rodríguez-Morgade, M. S.; Plonska-Brzezinska, M. E.; Athans, A. J.; Carbonell, E.; de Miguel, G.; Guldi, D. M.; Echegoyen, L.; Torres, T. *J. Am. Chem. Soc.* **2009**, *131*, 10484−10496. (c) Torres, T.; Gouloumis, A.; Sanchez-Garcia, D.; Jayawickramarajah, J.; Seitz, W.; Guldi, D. M.; Sessler, J. L. *Chem. Commun.* **2007**, *3*, 292−294.

(20) (a) Loi, M. A.; Denk, P.; Hoppe, H.; Neugebauer, H.; Meissner, D.; Winder, C.; Brabec, C. J.; Sariciftci, N. S.; Gouloumis, A.; Vazquez, P.; Torres, T. *Synth. Met.* **2003**, *137*, 1491−1492. (b) Neugebauer, H.; Loi, M. A.; Winder, C.; Sariciftci, N. S.; Cerullo, G.; Gouloumis, A.; Vázquez, P.; Torres, T. *Sol. Energy Mater. Sol. Cells* **2004**, *83*, 201−209. (c) Loi, M. A.; Denk, P.; Hoppe, H.; Neugebauer, H.; Winder, C.; Meissner, D.; Brabec, C.; Sariciftci, N. S.; Gouloumis, A.; Vázquez, P.; Torres, T. *J. Mater. Chem.* **2003**, *13*, 700−704. (d) Troshin, P. A.; Koeppe, R.; Peregudov, A. S.; Peregudova, S. M.; Egginger, M.; Lyubovskaya, R. N.; Sariciftci, N. S. *Chem. Mater.* **2007**, *19*, 5363−5372.

(21) (a) Rodríguez-Morgade, M. S.; Torres, T.; Atienza Castellanos, C.; Guldi, D. M. *J. Am. Chem. Soc.* **2006**, *128*, 15145−15148. (b) Jiménez, A. J.; Spänig, F.; Rodríguez-Morgade, M. S.; Ohkubo, K.; Fukuzumi, S.; Guldi, D. M.; Torres, T. *Org. Lett.* **2007**, *9*, 2481−2484. (c) Seitz, W.; Jiménez, A. J.; Carbonell, E.; Grimm, B.; Rodríguez-Morgade, M. S.; Guldi, D. M.; Torres, T. *Chem. Commun.* **2010**, *46*, 127−129. (d) Jiménez, A. J.; Grimm, B.; Gunderson, V. L.; Vagnini, M. T.; Calderon, S. K.; Rodríguez-Morgade, M. S.; Wasielewski, M. R.; Guldi, D. M.; Torres, T. *Chem. - Eur. J.* **2011**, *17*, 5024−5032. (e) Jimenez, A. J.; Sekita, M.; Caballero, E.; Marcos, M. L.; Rodríguez-Morgade, M. S.; Guldi, D. M.; Torres, T. *Chem. - Eur. J.* **2013**, *19*, 14506−14514. (f) Jimenez, A. J.; Calderon, R. M. C.; Rodriguez-Morgade, M. S.; Guldi, D. M.; Torres, T. *Chem. Sci.* **2013**, *4*, 1064−1074. (g) Sekita, M.; Jimenez, A. J.; Marcos, M. L.; Caballero, E.; Rodríguez-Morgade, M. S.; Guldi, D. M.; Torres, T. *Chem. - Eur. J.* **2015**, *21*, 19028−19040.

(22) (a) Fukuzumi, S.; Ohkubo, K.; Ortiz, J.; Gutierrez, A. M.; Fernández- Lazaro, F.; Sastre-Santos, A. *Chem. Commun.* **2005**, 3814−3816. (b) Li, X.; Sinks, L. E.; Rybtchinski, B.; Wasielewski, M. R. *J. Am. Chem. Soc.* **2004**, *126*, 10810−10811. (c) Chen, Y.; Lin, Y.; El-Khouly, M. E.; Zhuang, X.; Araki, Y.; Ito, O.; Zhang, W. *J. Phys. Chem. C* **2007**, *111*, 16096−16099. (d) Céspedes-Guirao, F. J.; Ohkubo, K.; Fukuzumi, S.; Sastre-Santos, A.; Fernandez-Lázaro, F. *J. Org. Chem.* **2009**, *74*, 5871−5880. (e) Céspedes-Guirao, F. J.; Ohkubo, K.; Fukuzumi, S.; Fernandez-Lázaro, F.; Sastre-Santos, A. *Chem. - Asian J.* **2011**, *6*, 3110−3121. (f) Céspedes-Guirao, F. J.; Martin-Gomis, L.; Ohkubo, K.; Fukuzumi, S.; Fernandez-Lázaro, F.; Sastre-Santos, A. *Chem. - Eur. J.* **2011**, *17*, 9153−9163. (g) Blas-Ferrando, V. M.; Ortiz, J.; Bouissane, L.; Ohkubo, K.; Fukuzumi, S.; Fernandez-Lazaro, F.; Sastre-Santos, A. *Chem. Commun.* **2012**, *48*, 6241−6243. (h) El-Khouly, M. E.; Gutierrez, A. M.; Sastre-Santos, A.; Fernandez-Lázaro, F.; Fukuzumi, S. *Phys. Chem. Chem. Phys.* **2012**, *14*, 3612−3621.

(23) (a) Würthner, F. *Chem. Commun.* **2004**, 1564−1579. (b) Mercadante, R.; Trsic, M.; Duff, J.; Aroca, R. *J. Mol. Struct.: THEOCHEM* **1997**, *394*, 215−226.

(24) Prodi, A.; Chiorboli, C.; Scandola, F.; Iengo, E.; Alessio, E.; Dobrawa, R.; Würthner, F. *J. Am. Chem. Soc.* **2005**, *127*, 1454−1462.

(25) (a) Barlow, S.; Marder, S. R. *Chem. Commun.* **2000**, *17*, 1555−1562. (b) Sandanayaka, A. S. D.; Sasabe, H.; Takata, T.; Ito, O. *J. Photochem. Photobiol., C* **2010**, *11*, 73−92.

(26) Vecchi, A.; Galloni, P.; Floris, B.; Dudkin, S. V.; Nemykin, V. N. *Coord. Chem. Rev.* **2015**, *291*, 95−171.

(27) See, for example: (a) Bandi, V.; El-Khouly, M. E.; Ohkubo, K.; Nesterov, V. N.; Zandler, M. E.; Fukuzumi, S.; D'Souza, F. *Chem. - Eur. J.* **2013**, *19*, 7221−7230. (b) Lim, G. N.; Webre, W. A.; D'Souza, F. *J. Porphyrins Phthalocyanines* **2015**, *19*, 270−280. (c) Lim, G. N.; Maligaspe, E.; Zandler, M. E.; D'Souza, F. *Chem. - Eur. J.* **2014**, *20*, 17089−17099. (d) Lee, S.-H.; Larsen, A. G.; Ohkubo, K.; Cai, Z.-L.; Reimers, J. R.; Fukuzumi, S.; Crossley, M. J. *Chem. Sci.* **2012**, *3*, 257−269. (e) Kelber, J. B.; Panjwani, N. A.; Wu, D.; Gomez-Bombarelli, R.; Lovett, B. W.; Morton, J. J. L.; Anderson, H. L. *Chem. Sci.* **2015**, *6*, 6468−6481.

(28) Lee, J. U.; Kim, Y. D.; Jo, J. W.; Kim, J. P.; Jo, W. H. *J. Mater. Chem.* **2011**, *21*, 17209−17218.

(29) Jin, Z.; Nolan, K.; McArthur, C. R.; Lever, A. B. P.; Leznoff, C. C. *J. Organomet. Chem.* **1994**, *468*, 205−212.

(30) Marcuccio, M. S.; Svirskaya, P. I.; Greenberg, S.; Lever, A. B. P.; Leznoff, C. C.; Tomer, B. *Can. J. Chem.* **1985**, *63*, 3057−3069.

(31) Rodríguez-Morgade, M. S.; Hanack, M. *Chem. - Eur. J.* **1997**, *3*, 1042−1051.

(32) Dokládalová, L.; Bureš, F.; Kuznik, W.; Kityk, I. V.; Wojciechowski, A.; Mikysek, T.; Almonasy, N.; Ramaiyan, M.; Padělková, Z.; Kulhánek, J.; Ludwig, M. *Org. Biomol. Chem.* **2014**, *12*, 5517−5527.

(33) Uchida, H.; Yoshiyama, H.; Reddy, P. Y.; Nakamura, S.; Toru, T. *Bull. Chem. Soc. Jpn.* **2004**, *77*, 1401−1404.

(34) Ahrens, M. J.; Sinks, L. E.; Rybtchinski, B.; Liu, W.; Jones, B. A.; Giaimo, J. M.; Gusev, A. V.; Goshe, A. J.; Tiede, D. M.; Wasielewski, M. R. *J. Am. Chem. Soc.* **2004**, *126*, 8284−8294.

(35) (a) Würthner, F.; Sautter, A.; Schilling, J. *J. Org. Chem.* **2002**, *67*, 3037−3044. (b) Panda, D. K.; Goodson, F. S.; Ray, S.; Lowell, R.; Saha, S. *Chem. Commun.* **2012**, *48*, 8775−8777.

(36) (a) Mak, C. C.; Bampos, N.; Darling, S. L.; Montalti, M.; Prodi, L.; Sanders, J. K. M. *J. Org. Chem.* **2001**, *66*, 4476−4486. (b) Webb, S. J.; Sanders, J. K. M. *Inorg. Chem.* **2000**, *39*, 5912−5919.

(37) (a) Cammidge, A. N.; Berber, G.; Chambrier, I.; Hough, P. W.; Cook, M. J. *Tetrahedron* **2005**, *61*, 4067−4074. (b) Berber, G.; Cammidge, A. N.; Chambrier, I.; Cook, M. J.; Hough, P. W. *Tetrahedron Lett.* **2003**, *44*, 5527−5529.

(38) (a) Thordarson, P. *Chem. Soc. Rev.* **2011**, *40*, 1305−1323. (b) Tsukube, H.; Furuta, H.; Odani, A.; Takeda, Y.; Kudo, Y.; Inoue, Y.; Liu, Y.; Sakamoto, H.; Kimura, K. In *Comprehensive Supramolecular Chemistry*; Atwood, J. L., Davies, J. E. D., MacNicol, D. D., Vögtle, F., Eds.; Pergamon: Oxford, 1996; Vol. *8*, No. 10, pp 425−482.

(39) (a) Frassineti, C.; Ghelli, S.; Gans, P.; Sabatini, A.; Moruzzi, M. S.; Vacca, A. *Anal. Biochem.* **1995**, *231*, 374−382. (b) Frassineti, C.; Alderighi, L.; Gans, P.; Sabatini, A.; Vacca, A.; Ghelli, S. *Anal. Bioanal. Chem.* **2003**, *376*, 1041−1052.

(40) Lowe, A. J.; Pfeffer, F. M.; Thordarson, P. *Supramol. Chem.* **2012**, *24*, 585−594.

(41) (a) Würthner, F.; Sautter, A.; Schmid, D.; Weber, P. J. A. *Chem. - Eur. J.* **2001**, *7*, 894−902. (b) Fukuzumi, S.; Ohkubo, K.; Ortíz, J.; Gutiérrez, A. M.; Fernández-Lázaro, F.; Sastre-Santos, A. *J. Phys. Chem. A* **2008**, *112*, 10744−10752.

(42) Nyokong, T.; Gasyna, Z.; Stillman, M. J. *Inorg. Chim. Acta* **1986**, *112*, 11−15.

DOI: 10.1021/jacs.6b07432
J. Am. Chem. Soc. 2016, 138, 12963−12974